Structural Behaviour of Composite RC Members Strengthened with UHPC Subjected to Static and Dynamic Loading

Hor YIN
Candidate for the Degree of Doctor of Philosophy
Supervisor: Assoc. Prof. Dr. Kazutaka SHIRAI
Division of Architectural and Structural Design

Introduction

Ultra-high performance concrete (UHPC) is a relatively new type of cementitious concrete materials. UHPC is a mix of reactive powder reaction (RPC) with steel fibres. Volume fractions of steel fibres of 1% to 5% are often used in the UHPC. UHPC can be defined by its high strength (> 150 MPa in compression and > 8 MPa in tension), high stiffness (Young's modulus of 45000 – 55000 MPa), extremely low permeability, and energy absorption. Due to its excellent properties, UHPC is often used in protective structures under aggressive environments and severe loadings such as earthquakes, impacts or blasts.

In addition, strengthening reinforced concrete (RC) members with UHPC can be an emerging technique for design, strengthening and protecting new or existing structures. Moreover, UHPC has shown high bond strength and good adherence to normal-strength concrete (NSC) substrates. Use of UHPC layer to strengthen the RC members has shown great potential in the enhancement of the structural performance.

However, investigation on the behaviour of composite UHPC-concrete members is very limited. Furthermore, research on non-composite UHPC structural members subjected to dynamic loading is relatively scarce, and dynamic response of composite UHPC-concrete members has not yet been performed in the previous literature.

In the present study, the investigation on the behaviour of composite UHPC-concrete members was conducted. This study could lead to further understanding the performance of the structural members under static and dynamic loading. This report is a summary of the author's doctoral dissertation.

Experiments

In this study, UHPC material was developed. Constituents of UHPC comprised cement, silica fume, quart powder, quart sand, river sand, water, superplasticizer, and steel fibres. After several trials, the best performance of UHPC mixture was chosen and used for the structural members. The material description and mix proportion are shown in Table 1.

Specimens conducted in this study are the rectangular slabs. A total of nine slabs with various UHPC configurations at the tension zone were tested. The test system and the section details are shown in Fig. 1.

Fig. 2(a) and (b) shows comparisons of load-midspan deflection curves from the test results for the specimens with rehabilitated UHPC, RE series, i.e. RE-20, RE-32, and RE-50, and with overlaid UHPC, OV series, i.e. OV-25, OV-25a, OV-50, and OV-50a, respectively.

As shown in Fig. 2(a), all UHPC-concrete composite slabs exhibited extensive deflection hardening and ductility during the post cracking range. Although no strength enhancement was attained in any of the strengthened slabs compared with specimen RE-0, it could easily be offset by their excellent energy absorption capabilities.

From Fig. 2(b), for OV series, owing to strengthening effect including the increase of the total height of the specimens, UHPC layer enhanced overall performance of UHPC-concrete composite specimens such as stiffness and ultimate load compared to specimen RE-0.

Fig. 3 shows typical crack patterns of the specimens after tests. All specimens strengthened with UHPC in RE series mainly failed in flexures. For OV series, all specimens failed in shear along with debonding of UHPC overlay.

Finite Element Modelling

- **Model description**

Finite element (FE) modelling was conducted using commercial software LS-DYNA. Concrete (NSC or UHPC) and reinforcing steels were modelled using an eight-node constant-stress solid element and a two-node beam element, respectively. A mesh size of 10 mm was used. A perfect bond was assumed between reinforcing steel and the concrete NSC or UHPC.

The effect of bond strength at the interface between UHPC and NSC substrate was considered for composite UHPC-concrete specimens. The bond interface was modelled using equivalent beam elements at the interface. The equivalent beam elements were created at all nodes of the cross-sectional interface and extruded along the longitudinal specimen axis. The detail of the FE model with the equivalent beam elements is illustrated in Fig. 4.

- **Material models**

In the present study, the concrete damage model or Mat-72r3 in LS-DYNA was employed for both the NSC and UHPC. For reinforcing steels, a material model (Mat-03 in LS-DYNA), which is an elastic-plastic model with kinematic and isotropic hardening, was used. For accuracy of the developed FE mode, the strain rate effect, which is defined by dynamic increased factor (DIF), was not considered in the numerical simulations for the materials.

For the equivalent beam elements, an elastic-plastic characteristic was adopted, and Mat-03 in LS-DYNA was used. The equivalent bond strength $f_{y,eb}$ and Young's modulus E_{eb} were defined based on the weak concrete NSC.

Table 1. UHPC material properties

Constituent	Description	Mix proportion by weight
Cement	Ordinary Portland cement Type I	1.00
Silica fume	Bulk density is 204.4 kg/m^3	0.25
Quartz powder	Minimum 97% pass through 325 mesh sieve	0.25
Quartz sand	P100/300 minimum 80% retained	0.48
River sand	0.3 – 0.8 mm	0.80
Water/Cement ratio	-	0.20
Superplasticiser	Sika ViscoCrete 2044	0.05
Steel fibre (%Vol.)	Straight fibres 13 mm long, 0.2 mm diameter, tensile strength > 2300 MPa	3%

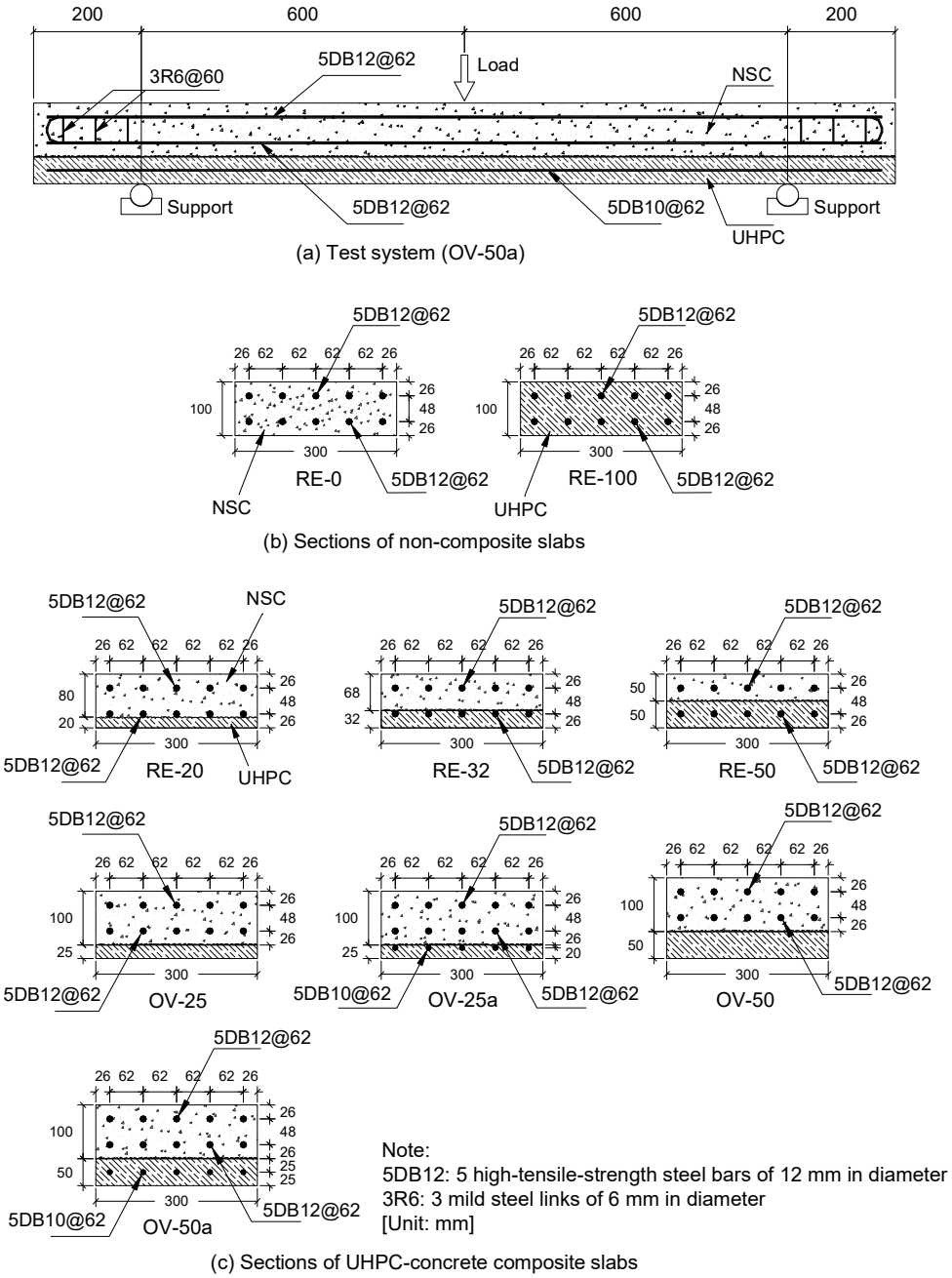

Fig. 1. Geometric details of composite UHPC-concrete slabs.

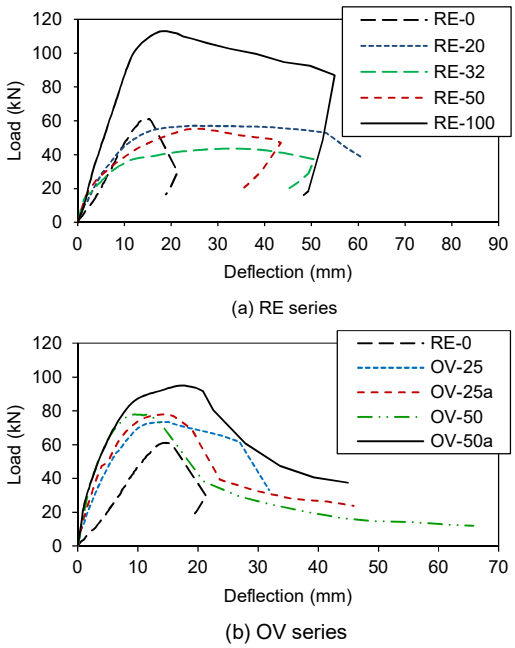

Fig. 2. Load-midspan deflection curves of the test specimens.

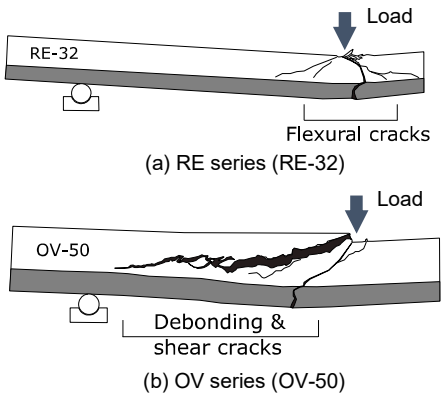

Fig. 3. Typical crack patterns observed from the tests.

- **Loadings**

A static loading was applied directly to the nodes at the midspan of the specimens, and the displacement-controlled loading was used. An implicit method, which usually suitable for static analysis, and a loading rate of 2×10^{-5} m/s were adopted for all the specimens. However, an explicit method was also employed for particular specimens for the sake of comparisons. Because the explicit method generally requires smaller time steps than do the implicit method, and thus leads to longer computational time for the static event, to shorten the simulation time in explicit method, an increase of loading rate of 2×10^{-3} m/s was adopted.

For dynamic behaviour, blast simulations were conducted. Blast loading was modelled using built-in algorithm load-blast-enhanced function. The major advantage of this function is that it can avoid the detailed modelling of the explosive charge and shock wave in air. The function requires only the equivalent mass of TNT, location of the detonation charge, and type of blast. The blast type used in the present study was the spherical free-air burst (default in LS-DYNA).

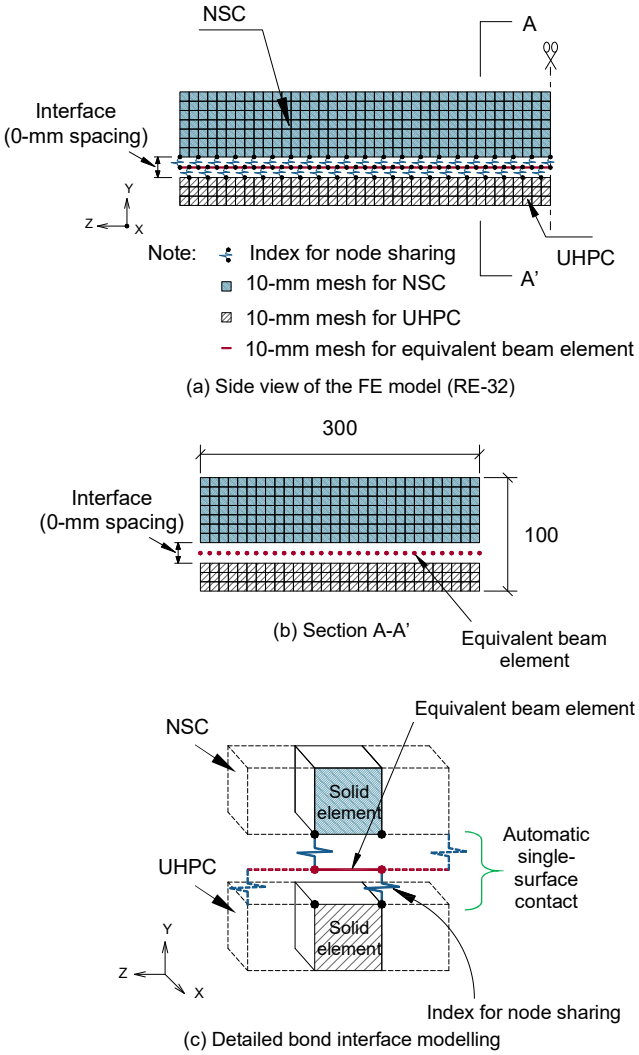

Fig. 4. Details of FE modelling.

- **Simulation results under static loading**

The experimental and numerical peak loads P_{exp} and P_{FEM} and the corresponding midspan deflections Δ_{exp} and Δ_{FEM} were obtained and compared. The experimental-to-numerical peak load ratio P_{exp}/P_{FEM} and the corresponding peak load deflection ratio $\Delta_{exp}/\Delta_{FEM}$ were also calculated, and the results are given in Table 2. From Table 2, the numerical peak loads showed a good accuracy with average P_{exp}/P_{FEM} ratio and coefficient of variation (COV) of 0.99 and 4.4%, respectively. For the corresponding midspan deflection, fair agreement was obtained with average $\Delta_{exp}/\Delta_{FEM}$ ratio and COV of 1.27 and 35.0%, respectively.

In addition, numerical results from the explicit method were obtained and compared with those from the implicit method and experiments. Configurations of the effective plastic strain obtained from the numerical simulations are shown in Fig. 5, which were roughly in good correlation with the experimental crack pattern after test. Moreover, the load-deflection curves extracted from the implicit and explicit method showed similar performance and agreed well with the experimental results as shown in Fig. 6. It should be mentioned that the FE model using implicit and explicit method was calibrated individually. The model calibration based on the explicit method was intended to

Table 2. Simulated peak load and the corresponding midspan deflection

Type	Specimen	P_{exp} (kN)	P_{FEM} (kN)	Δ_{exp} (mm)	Δ_{FEM} (mm)	P_{exp}/P_{FEM} -	$\Delta_{exp}/\Delta_{FEM}$ -
Non-composite	RE-0	61.08	64.03	14.79	15.15	0.95	0.98
	RE-100	113.05	109.88	18.14	27.05	1.03	0.67
UHPC-concrete composite	RE-20	57.18	60.38	24.59	13.82	0.95	1.78
	RE-32	43.68	42.85	31.12	22.55	1.02	1.38
	RE-50	55.38	52.19	25.68	30.47	1.06	0.84
	OV-25	73.47	71.52	13.78	11.97	1.03	1.15
	OV-25a	77.97	81.77	14.42	9.32	0.95	1.55
	OV-50	77.97	82.52	9.43	8.86	0.94	1.06
	OV-50a	95.06	94.68	17.75	8.854	1.00	2.00
Average						**0.99**	**1.27**
Coefficient of variation (COV)						**4.4%**	**35.0%**

Note: P_{exp} = the experimental peak load; P_{FEM} = the numerical peak load; Δ_{exp} = midspan deflection corresponding to the experimental peak load; and Δ_{FEM} = midspan deflection corresponding to the numerical peak load

use for the dynamic behaviour of composite UHPC-concrete members under blast loading as described in the following section.

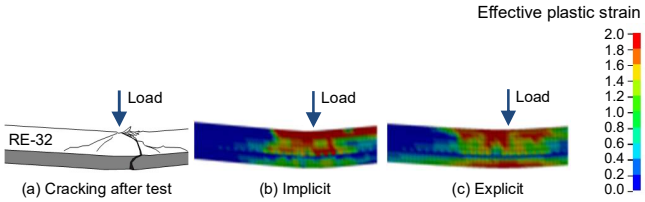

Fig. 5. Simulated damage configurations versus experimental crack pattern (RE-32).

- **Simulation results under blast loading**

The dynamic behaviour of composite UHPC-concrete members subjected to blast loading was numerically investigated using explicit method. The numerical simulations of composite RC members strengthened with different UHPC configurations were carried out by varying the blast charge weight. The blast simulation was based on the equal model parameters developed using explicit method for static behaviour. An assumed damping ratio of 5% was used to consider the damping effect of the blast response. Fig. 7 shows the overview of the FE model for blast simulations.

Figs. 8 and 9 compare the simulated deflection-time histories of the composite UHPC-concrete specimens with those of non-composite NSC specimen RE-0 and UHPC specimen RE-100. It showed that UHPC layer significantly improves the blast resistance compared to that of RE-0.

In addition, two other simulations on reversed composite UHPC-concrete specimens, $(RE\text{-}32)_{REV}$ and $(OV\text{-}50)_{REV}$, were also conducted. These investigations could reflect the effect of UHPC strengthening layer subjected to blasting in comparison to the respective blast response of the NSC component of the composites. The simulated deflection-time curves showed that the UHPC layer of $(RE\text{-}32)_{REV}$ and $(OV\text{-}50)_{REV}$, could serve a better improvement of the blast response as seen in Figs. 10 and 11.

Based on the numerical results, it could be concluded that use of UHPC strengthening layer can mitigate the blast effect on dynamic response of composite UHPC-concrete members.

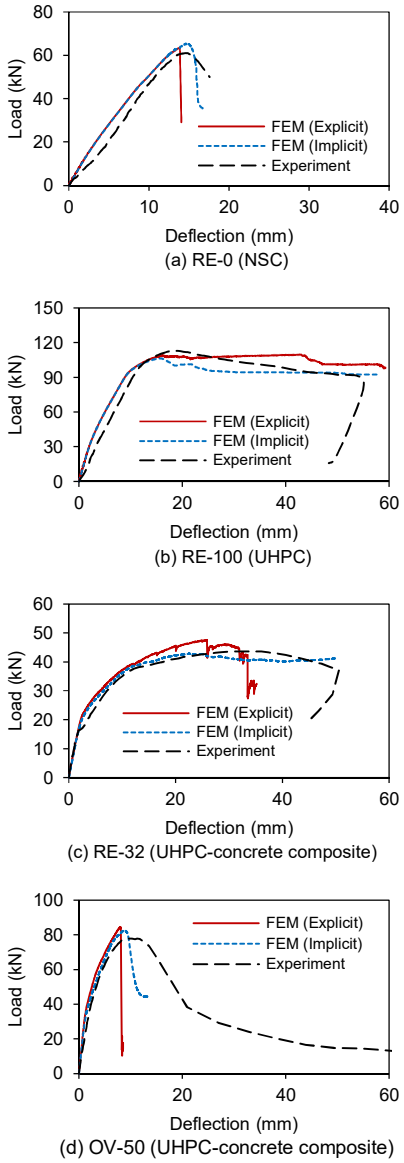

Fig. 6. Load-deflection curves under static loading.

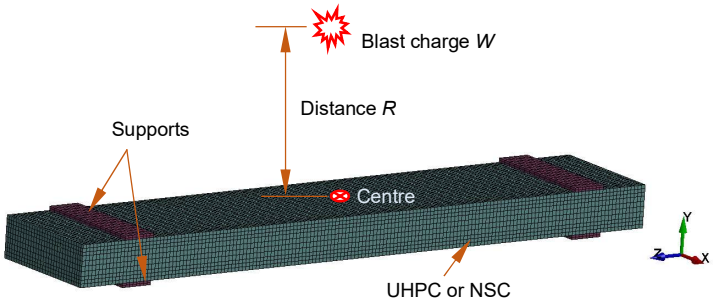

Fig. 7. Configuration of FE model for blast simulation.

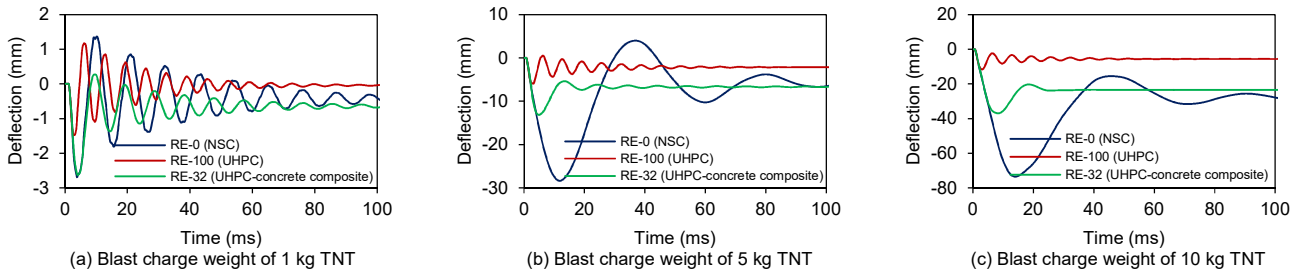

Fig. 8. Comparisons of simulated deflection-time histories for UHPC-concrete composite specimen RE-32, and non-composite specimens RE-0 (NSC) and RE-100 (UHPC).

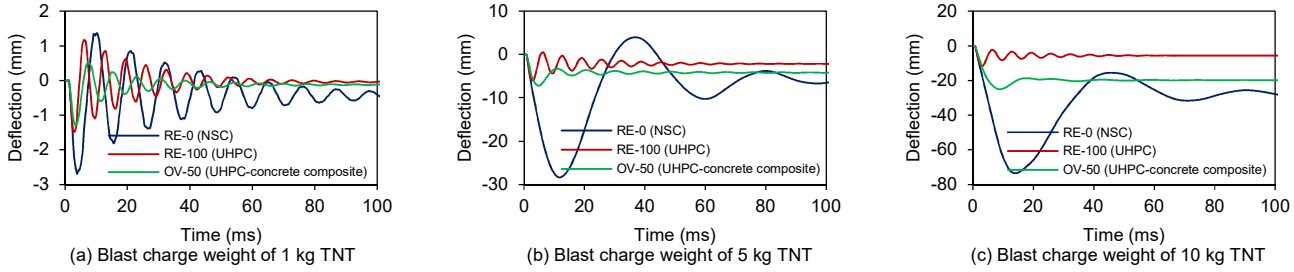

Fig. 9. Comparisons of simulated deflection-time histories for UHPC-concrete composite specimen OV-50, and non-composite specimens RE-0 (NSC) and RE-100 (UHPC).

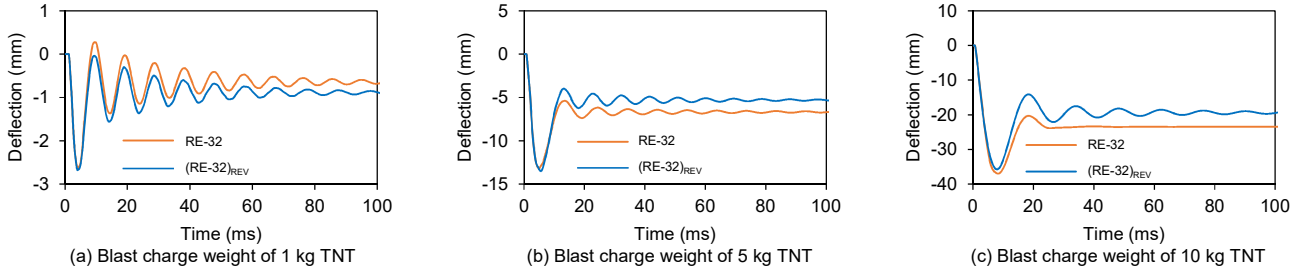

Fig. 10. Comparisons of simulated deflection-time histories of RE-32 and $(RE\text{-}32)_{REV}$.

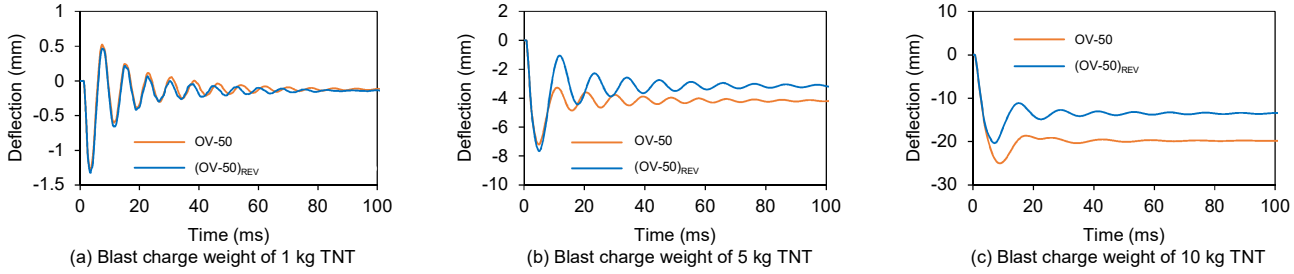

Fig. 11. Comparisons of simulated deflection-time histories of OV-50 and $(OV\text{-}50)_{REV}$.

Prediction of Structural Capacity

- **Capacity of composite UHPC-concrete members**

To date, no design codes have been made available for the prediction of the capacity of the composite UHPC-concrete members. Methods that can be used to calculate the flexural and shear strength are therefore needed. Applications based on the existing design models of RC or fibre reinforced concrete (FRC) structures could be useful because they are simple and easy to use.

For this purpose, the present study introduces methods of predicting the flexural and shear strength of composite UHPC-concrete members based on the existing design models. In the flexural strength calculation, the compressive and tensile stresses was assumed as simplified rectangular stress blocks for the NSC and UHPC, respectively. Fig. 12 shows the representation of the assumed stresses and strains in the composite UHPC-concrete section. For shear strength prediction, six independent methods were adopted. Three of them (Methods A1, A2, and A3) were based on the conversion of the volume fraction of steel fibres in the UHPC in an equivalent longitudinal steel ratio. The other three methods (Methods B1, B2, and B3) involved the computation of the shear strength as a sum of the contributions ot the shear strength by the RC member and the UHPC layer, each of which is independently calculated. Methods B1, B2, and B3 were adopted for the sake of simplicity and to allow comparison with the other methods.

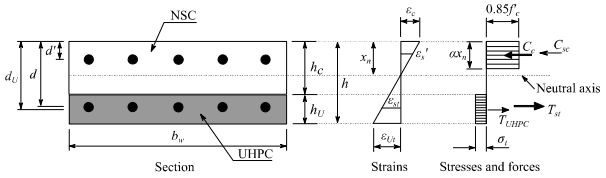

Fig. 12. Calculation assumptions for flexural strength of composite UHPC-concrete members.

- **Prediction results**

In this report, the flexural strength calculation results for the RE series was obtained and compared with the test results as shown in Fig. 12, and no shear strength was presented because the specimens were mainly failed in flexure. Likewise, the shear strength prediction for the OV series was shown in Fig. 13, and no flexural strength was reported because the specimens failed in shear.

As can be observed in Figs. 12 and 13, the proposed methods based on the modification of existing design models were able to predict the capacity of composite UHPC-concrete member with reasonable accuracy.

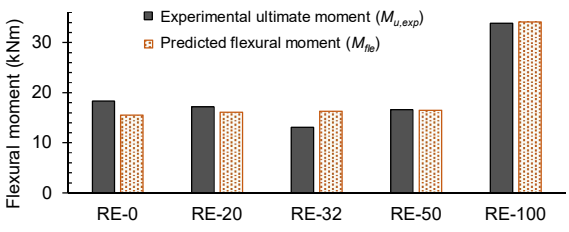

Fig. 12. Flexural moment (RE series).

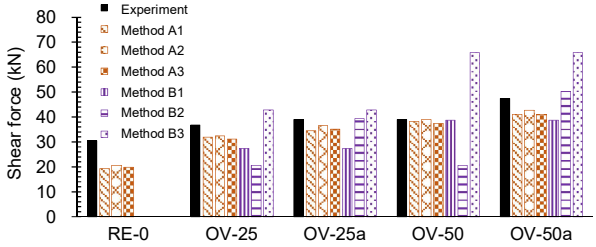

Fig. 13. Shear strength (OV series).

Summary

The static and dynamic behaviour of composite RC members strengthened with UHPC was investigated.

From the experimental observation, the UHPC layer helps enhance the structural performance of composite UHPC-concrete members. Moreover, the developed FE model was able to accurately predict the behaviour of the composite members.

For dynamic behaviour, blast simulations were conducted to investigate the influence of UHPC strengthening layer on the blast resistance of UHPC-concrete members. It showed that UHPC layer could be used to mitigate the blast effect.

Calculation methods of the structural capacity of composite UHPC-concrete members were proposed. The prediction results showed very promising.

This study could help the development of design codes for composite UHPC-concrete structural members in the future.

Publications

- **International peer-reviewed journal**

Hor Yin, Wee Teo, Kazutaka Shirai, "Experimental investigation on the behaviour of reinforced concrete slabs strengthened with ultra-high performance concrete," *Constr Build Mater*, 155, 463–474, 2017. IF=3.169

- **Peer-reviewed conference proceedings**

Hor Yin, Kazutaka Shirai, Wee Teo, "Shear capacity prediction of reinforced concrete members strengthened with ultra-high performance concrete overlay," In: *Proceedings of the Japan Concrete Institute*, 40, 2018.

Kazutaka Shirai, **Hor Yin**, Wee Teo, "Flexural strength calculation of the RC members rehabilitated with UHPC," In: *Proceedings of the Japan Concrete Institute*, 40, 2018.

Hor Yin, Kazutaka Shirai, Wee Teo, "Numerical assessment of ultra-high performance concrete material," *2016 IEEE International Conference on Innovative Engineering Materials (ICIEM 2016)*, Singapore, August 20–22, 2016. (Online open: IOP Conference Series, Mater Sci Eng, 241, 2017, 012004)

Hor Yin, Kazutaka Shirai, Wee Teo, "Response of UHPC-concrete composite structural members using implicit and explicit finite element method," *2018 The 3rd International Conference on Advanced Functional Materials (ICAFM 2018)*, San Francisco, USA, August 3–5, 2018. (Accepted)